High Curie Temperature CoSi nanowires by Mn-doping.

Ángel R. Ruiz,[1] José Hernández-Pérez,[1] Luis F. Fonseca,[1] Miguel José Yacamán,[2] Eduardo Ortega,[2] and Arturo Ponce,[2]

[1]*Department of Physics, University of Puerto Rico – Río Piedras Campus, San Juan, Puerto Rico 00692, Puerto Rico.*

[2]*Department of Physics and Astronomy, University of Texas at San Antonio, San Antonio, Texas 78249, USA.*

We report the synthesis of high Curie temperature (T_C >800K) Mn-doped CoSi nanowires. CoSi and $Co_{1-x}Mn_xSi$ nanowires were synthesized by Chemical Vapor Deposition. Transmission electron microscopy was used to identify a crystalline B20 cubical structure. Zero-field cooling and field cooling measurements confirm a spin disorder behaviour at low temperatures. The magnetic properties of doped samples were explained by means of the Ruderman-Kittel-Kasuya-Yosida (RKKY) interaction where the localized Mn atoms interact with the conduction electrons in CoSi providing a net ferromagnetic moment and explaining spin disorder at low temperatures. An individual CoSi nanowire was experimentally analysed by performing off-axis electron holography, providing information about its local magnetization. DFT calculations were performed to understand the effects of Mn doping, Si-vacancies, and surface atoms in the magnetic properties at the surface of the nanowire. An estimation of the Curie temperature was made using the mean field approximation (MFA).

I. INTRODUCTION

The integration of magnetic metallic components on the top of conventional silicon circuits have been proposed to be a key feature in the making of new spin electronic (or spintronic) systems as an improvement to current electronic technology [1]. Nanostructured transition metal mono-silicide nanowires have shown encouraging magnetic properties at different temperatures. For example, manganese silicide nanowires (MnSi) present helimagnetic states below 30K [2] and cobalt silicide nanowires (CoSi) are ferromagnetic at room temperature [3]. The doping with transition metals of these mono-silicides also has caught the attention due to the enhancement of their magnetic properties. For instance, iron Silicide (FeSi) nanowires are reported as a paramagnetic material [4] but its counterpart; cobalt-doped FeSi ($Fe_{1-x}Co_xSi$) exhibits a Curie temperature close to 38 K [5] when synthesized as nanowires. In addition, manganese-doped FeSi ($Fe_{1-x}Mn_xSi$) nanowires possess remnant magnetization at room temperature [6], enhancing their ferromagnetic properties even further.

It has been demonstrated recently that Co_2MnSi present half metallicity at room temperature, featuring a high Curie temperature about 1000K [7] and chemical stability due to its Heusler phase. However, the replacement of a Mn atom for a Co one in bulk MnSi ($Mn_{1-x}Co_xSi$) have shown a suppression of the helimagnetic phase transition presented at low temperature in MnSi [8]. Little is known about the magnetic properties of Co_xMn_ySi in the nanoscale form. Model calculations have attributed the magnetism of nanoscale CoSi to the presence of Si vacancies that enhances the

magnetic moment of Co atoms[9]. In the best of our knowledge, the effect of Si vacancies on Mn surface atoms in $Co_{1-x}Mn_xSi$ (CoMnSi) nanowires has not been reported. Here we report the synthesis of CoMnSi nanowires by chemical vapor deposition (CVD) and their promising magnetic properties. Model calculations are discussed that help to understand the role of Si vacancies and Mn doping on the observed increase of the total magnetic moment.

Nanowires have been chosen as the subject of this study due to their inherent shape anisotropy. As a consequence, ferromagnetic nanowires exhibit unique and tunable magnetic properties, very different to their bulk and thin film counterparts [10]. Based on the shape anisotropy and orientation assembly, Co nanowires show a high temperature coercivity about 10.6 kOe [11]. In addition, magnetic nanowires are promising candidates for 3D magnetic memory devices with small footprint. [12,13]

II. EXPERIMENTAL

CoMnSi and CoSi nanowires were synthesized in a CVD reactor. The CVD synthesis of CoSi nanowires have been previously reported by several authors[3,14-18]. The synthesis approach was based on the well-known Arkel method, which separates the metal through vapor transport [19]. Following previous reports, the metal halide precursor was placed inside a quartz tube at the upstream zone of a conventional two-zones horizontal hot-wall furnace. Once the gaseous state is reached, the precursors are transported with a 400 sccm Ar flux towards a Si (111) substrate, previously washed and etched using a 10% hydrofluoric acid solution and placed at the downstream zone. For the synthesis of CoSi nanowires the Si substrate temperature was set to 950 °C (oven thermocouple reading) in the downstream zone, where the gaseous precursor reacted with the Si substrate to form the free-standing nanowires. The pressure was kept at 500 Torr. Anhydrous $CoCl_2$ (Alfa Aesar) was used as a cobalt precursor. The absence of metal catalysts at the tip of the synthesized nanowires supports the self-assembly of nanowires by a vapor-solid mechanism. The pathways for $CoCl_2$ vapor to react with Si at the substrate have been proposed elsewhere [3]:

$2CoCl_2(g)+3Si(s) \leftrightarrow 2CoSi(s) + SiCl_4(g)$

$CoCl_2(g)+SiCl_4(g) \leftrightarrow CoSi(s) + 3Cl_2(g)$

The Mn-doping was promoted by placing anhydrous $MnCl_2$ (Alfa Aesar) at the upstream zone to perform a chemical reaction that produces the CoMnSi nanowires. For the formation of CoMnSi nanowires the downstream temperature was set to 900 °C and a pressure of 1 atm. When the thermodynamic conditions have been reached, the gaseous $CoCl_2$ and $MnCl_2$ precursors could react in the two following ways with the Si substrate to form the CoMnSi nanowires:

$2(Mn,Co)Cl_{2(g)} + 3Si_s \rightarrow 2Co_{1-x}Mn_xSi_{(s)} + SiCl_{4(g)}$

$SiCl_{4(g)} + (Mn,Co)Cl_{(2g)} \rightarrow Co_{1-x}Mn_xSi_{(s)} + 3Cl_{2(g)}$

Direct measurements of standard enthalpies of formation of the silicides show that the exothermic reaction favors the formation of CoSi over its counterpart MnSi by having lower enthalpy than MnSi [20], with the additional fact that the enthalpy of formation of the $MnCl_2$ is lower than $CoCl_2$. These factors together contribute to the formation of CoMnSi nanowires, more energetically favorable than $Mn_xCo_{1-x}Si$. Because the mono silicide forms with the same equilibrium structure as its other analogue MnSi, the chemical substitution of Co at the transition metal site is easily accomplished giving rise to the Mn-doped CoSi nanowires.[21] In both cases (CoSi and CoMnSi) the synthesis produced high yields of nanowires as shown in figures 1a and 1b.

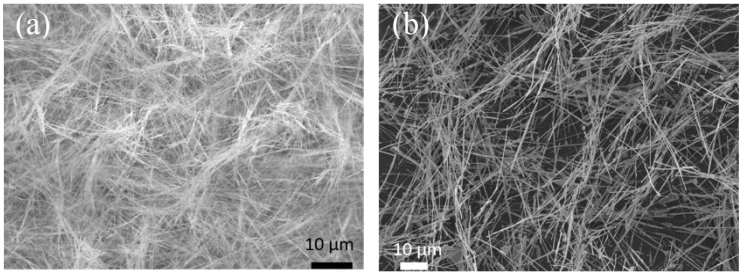

Fig. 1 SEM images of as-grown: (a) CoSi nanowires and (b) CoMnSi nanowires on Si substrates.

III. RESULTS AND DISCUSSION

Chemical and structural characterization of the nanowires have been performed by transmission electron microscopy (TEM) and analytical techniques such as energy-dispersive X-ray spectrometry (EDS), electron diffraction, and X-Ray diffraction (XRD). TEM was performed in a JEOL 2010F microscope operated at 200 kV and XRD using a Rigaku X-Ray diffractometer with Cu-K alpha radiation. The diameter measured in as grown CoSi and CoMnSi nanowires ranges from 50 nm to 500 nm as shown in Figure 2a and Figure 3a, respectively. Selected area electron diffraction (SAED) patterns, and high-resolution transmission electron microscopy (HRTEM) measurements show a cubic crystalline structure space group $P2_13$ in both, CoSi and CoMnSi nanowires. HRTEM and SAED show a preferred growth direction along the [2 1 1] direction in CoSi nanowires as shown in Fig. 2a,b,c. Figure 2b indicates interplanar spacing of the lattice in HRTEM image and its fast Fourier transform (FFT) inset. CoMnSi measurements suggest a polycrystalline nature. Elemental analyses performed by EDS are shown in Figure 2d for CoSi and Figure 3c for CoMnSi, the later shows the presence of Mn with an approximated concentration of 3%. The XRD patterns (Figure 2e and Figure 3d) confirm the crystalline cubic structures space group $P2_13$ in CoSi and CoMnSi nanowires. XRD patterns were compared with CoSi and $CoSi_2$ structures; these patterns match with the CoSi cubic structure (lattice constant 4.43 Å), in which the highest peak corresponds to the (210) peak followed by the second highest peak (211) as shown in Figure 2e and 3d. HRTEM and SAED measurements on the Mn-doped nanowires

(Figures 3a and 3b) show polycrystalline growing compared with the CoSi nanowires and a SiO_x amorphous coating layer in both, CoSi and CoMnSi.

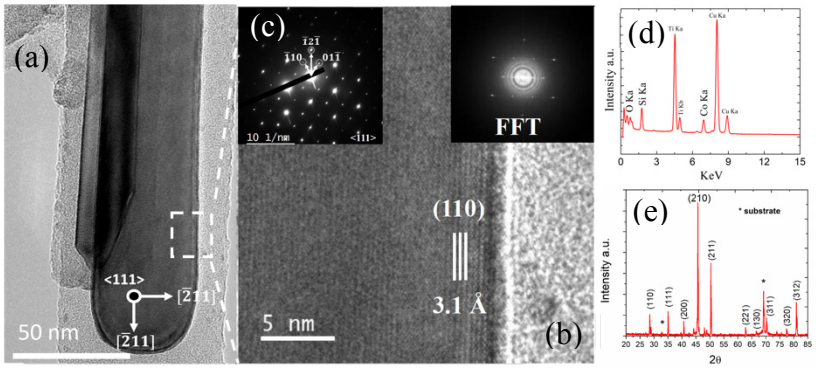

FIG.2. TEM image of a single CoSi nanowire, (b) HRTEM image of the region selected in (a) indicating planes, (c) SAED pattern registered close to the <111> zone axis. The labeled distance corresponds to the $(0,\bar{1},2)$ planes. d,e) EDS and XRD characterization demonstrate the 1:1 nature of the material and confirms the B20 cubic crystalline structure. The Ti peak is due to the TEM holder.

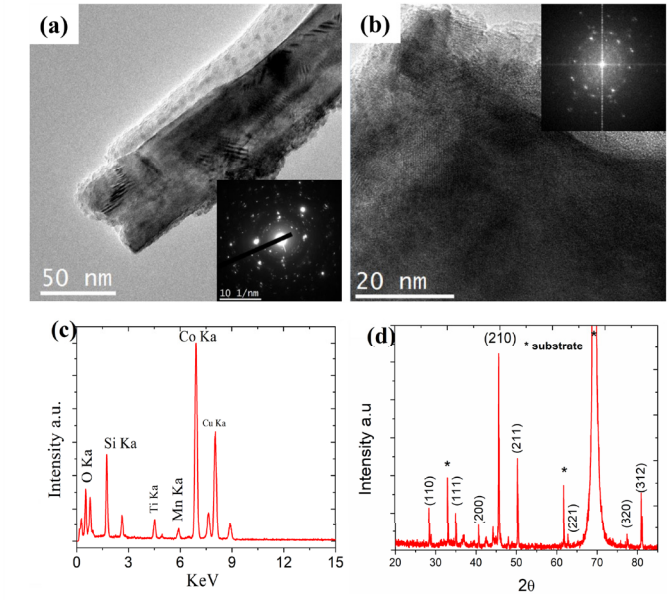

FIG. 3. (a) TEM image of a single CoMnSi nanowire and SAED inset, (b) HRTEM image and FFT inset. (c) EDS and (d) XRD pattern. The Ti peak is due to the TEM holder

The magnetic properties of the as-grown CoMnSi and CoSi nanowires were measured using a Physical Property Measurement System (PPMS) magnetometer. Results in Figure 4 show the nanowire's magnetization at different temperatures as a function of the external magnetic field. The magnetic contribution of the Si substrate is 10^{-06} emu[3], thus can be ignored. Both materials exhibit ferromagnetism at room temperature, while CoMnSi exhibits ferromagnetism at temperatures higher than 800K, as its counterpart, the Heusler alloy Co_2MnSi. Figure 4a shows the hysteresis curves of CoSi and CoMnSi nanowires at 300K and at 800K for CoMnSi. Figure 4b presents Field Cooling (FC) and Zero-Field Cooling (ZFC) measurements for CoMnSi. CoMnSi presents a spin freeze like behavior by increasing its magnetic moment with temperature until the material reaches ~300K. The difference in figure 4b between the magnitudes of the magnetic moment at 400 K in CoMnSi is due to the conditions in which the two experiments (low temperature and high temperature) were performed. From 4K- to 400K (low temperature), the nanowires were previously magnetized to measure the hysteresis loop at 300K (fig 4a). From 400K-800K (high temperature) the materials were already demagnetized. This can also be seen in the FC measurements from 800K-400K where the materials underwent a hysteresis loop at 800K.

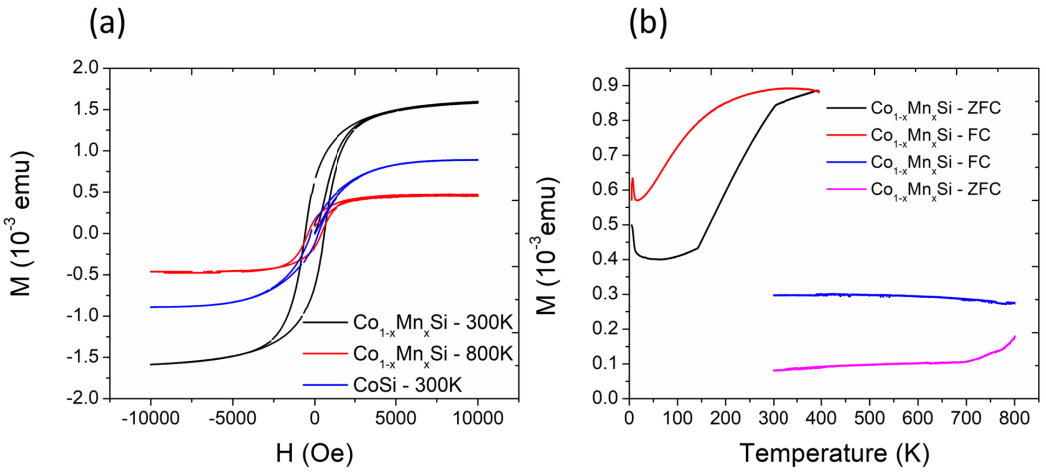

FIG. 4. a) Magnetic hysteresis of CoSi and CoMnSi nanowires. Both materials exhibit ferromagnetism above room temperature. b) ZFC and FC measurements for CoMnSi nanowires. Spin disorder can be observed at low temperatures.

It has been proposed that the origin of magnetism in CoSi nanowires is the formation of ordered vacancies which enhance the magnetic moment of the Co atoms placed at the surface[9]. Recent studies on Ta-doped TiO_2 suggest the formation of Ti vacancies induced by Ta doping, forming a localized magnetic moment around the Ti vacancies [22]. Thereby the origin of the magnetism on these CoMnSi nanowires could be due to the itinerant Mn electrons around the Si vacancies, which interact with the conduction electrons of the neighboring cobalt atoms, also explaining the spin freeze behavior at low temperatures. Such mediated exchange can be explained by the Ruderman-Kittel-Kasuya-Yosida (RKKY) interaction.

Following RKKY approach [23,24] for the ferromagnetic case, the total magnetic contribution of the conduction electrons induced by an external magnetic field can be expressed in the form of:

$$\mathcal{H}_{exchange} = -\frac{JN_e}{N} \boldsymbol{s} \cdot \boldsymbol{S}\,, \qquad (1)$$

where N_e /N is the number of electrons per unit cell, S is the localized spin of the impurity atoms, s represents the spin of the conduction electrons and J is the exchange interaction constant.

In the RKKY for dilute alloys, the Mn atoms occupy random points in the lattice, differing their internal magnetic moment by magnitude and direction[18,19]. Below the spin freezing temperature, the Mn spins are "frozen" in their randomly oriented direction. This behavior could be observed at low temperatures in CoSi nanowires as reported by Kwanyong et al[3]. The author attributed their M-T curve divergence to uncoordinated Co atoms at the surface. Similarly, our nanowires experience a small divergence at low temperature (T<20K) followed by the M-T measurements convergence at higher temperature as shown in Figure 4b. This behavior is observed in other transition metal alloys. Work on $Fe_{3-x}Mn_xSi$ alloys have shown spin glass like behavior proportional to the Mn concentration [25]. In addition, the critical point in which the material changes its phase from spin glass to ferromagnetic or paramagnetic depends both on temperature and concentration. High concentration (20%-80%) favors a spin glass–paramagnetic transition as shown by Yeshurun et al. on Fe-Mn alloys [26]. The ZFC and FC measurements converge at room temperature where the hysteresis loop presents a room temperature ferromagnetic material. High temperature measurements suggest that the system could still be experiencing some spin disorder at low fields. Because HRTEM, XRD and EDS measurements indicate a highly crystalline (polycrystalline) Mn-doped material, we consider that the origin of ferromagnetism on the CoMnSi nanowires is the uncoordinated Mn atoms through the surface of the nanowire (where disorder is favored) and not due to strains or structural defects within the nanowire.

To have a deeper insight of the magnetic properties of the Co and Mn atoms in both materials (CoSi and CoMnSi) and to ensure that the Si atoms do not contribute with a net magnetic moment within the nanowires, spin polarized density functional theory (DFT) calculations were performed using the Vienna Ab initio Simulation Package (VASP)[27-29]. To have the closest configuration to the real systems a (0 -1 1) slab was considered. Two supercells of 20 Co and 18 Si atoms were built with two ordered vacancies on the surface (Figure 5). Another supercell of 20 Co and 20 Si atoms was also built to compare the effects of ordered vacancies in the magnetization of the Co atoms. For the calculations, the many-body LDA approximation was implemented with the projector augmented wave (PAW) [30]. The energy cut-off for the plane wave expansion was 300 eV. The Brillouin zones were sampled in a gamma-centred grid with a k-point mesh of 8 x 8 x 1. Figure 6 gives the local magnetic moments of Co and Si atoms for the chosen configurations.

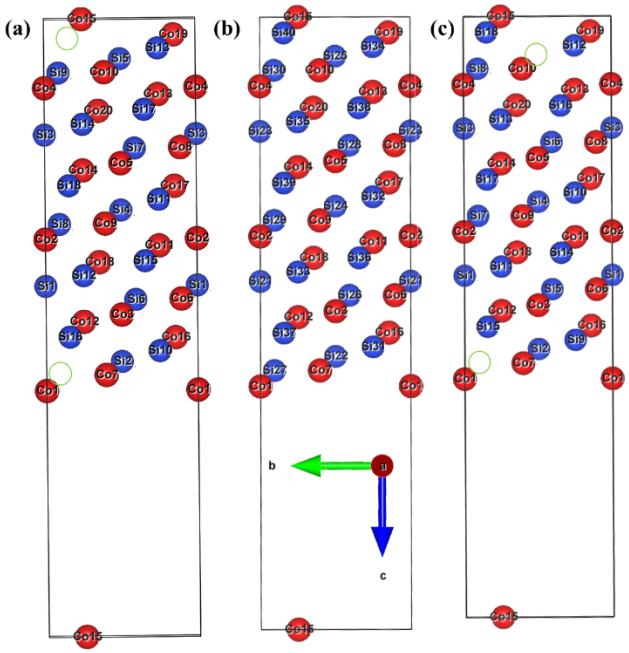

FIG. 5. Supercell configurations used for the DFT calculations. a) The labeled 40 and 27 Si atoms were removed. This configuration gave the highest magnetic moment for the considered configurations. b) The original configuration without the Si vacancies. c) The labeled 25 and 27 Si atoms were removed. This configuration gave a Curie temperature above room temperature**.** Total magnetic moment for each configuration can be seen in Figure 6.

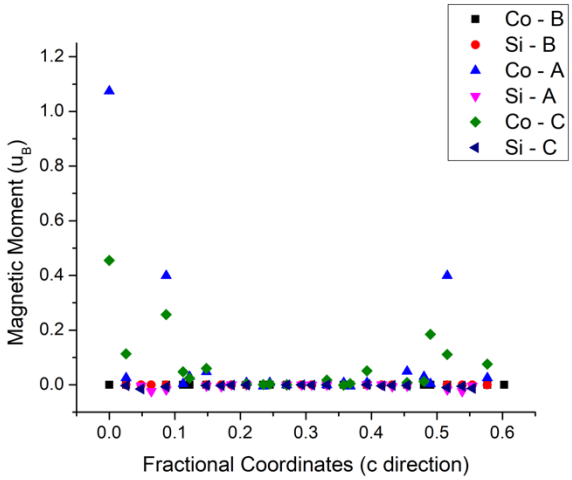

FIG. 6. Calculated magnetic moments of Co and Si atoms in the (0 -1 1) slab. The boundaries are taken with the cobalt atoms labelled as 15 and 1 in Figure 5 with position 0 and 0.60268, respectively. Label A and C correspond to supercells with two Si vacancies at the surface (one vacancy at each end of the supercell). Label B corresponds to the supercell without vacancies.

For the estimation of the Curie temperature we chose an in-plane alignment for the antiferromagnetic coupling between Co atoms (Figure 7).

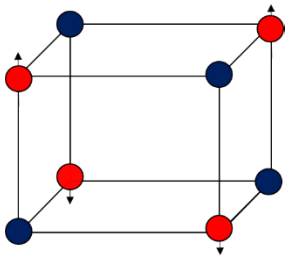

FIG. 7**.** In-plane antiferromagnetic coupling between Co atoms in CoSi unit cell. Co atoms labelled as red and Si atoms labelled as black.

Similarly to recent studies on MnSi [31], the magnetism of the CoSi nanowires can be explained by means of a direct exchange interaction between the magnetic cobalt atoms by means of a generalization of the Heisenberg Hamiltonian. Having the antiferromagnetic ground state energy, with the molecular field theory (MFA) approximation we can estimate the Curie temperature for a direct exchange between Cobalt atoms in the undoped case as:

$$\boldsymbol{T_c = \frac{2JS(S+1)}{3k_B}} \qquad (2)$$

Where k_B is the Boltzmann constant. The ground state energy difference between magnetic states is given by:

$$\boldsymbol{E_\downarrow - E_\uparrow = N_\downarrow JS_z^2 + N_\uparrow JS_z^2}, \qquad (3)$$

where $\boldsymbol{N_\downarrow}$ and $\boldsymbol{N_\uparrow}$ are the number of first nearest neighbors for the antiferromagnetic and ferromagnetic configurations, respectively. The ferromagnetic configuration has a total of 6 neighbors while the antiferromagnetic has 3 neighbors and because each magnetic interaction *J* involves two magnetic centers[32], our energy difference reduces to:

$$\boldsymbol{E_\downarrow - E_\uparrow = \frac{9}{2}S_z^2 J \Rightarrow J = \frac{2}{9S_z^2}E_\downarrow - E_\uparrow}$$

Hence the final expression for the Curie temperature for a direct exchange between Co atoms in CoSi could be written in the form:

$$\boldsymbol{T_c = \frac{4(1+\frac{1}{S_z})(E_\downarrow - E_\uparrow)}{27 * 8.617\times10^{-05} eV \cdot K^{-1}} = \frac{E_\downarrow - E_\uparrow}{1.045\times10^{-03} eVK^{-1}}}$$

where $S_z = 3/2$ for cobalt.

For CoMnSi, there is one Co and Si atom per unit cell, hence, the total number of valence electrons per unit cell is 5. The spin magnetic moment for Mn is 5/2. Similarly:

$$T_c = \frac{7J}{15k_B} = \frac{(E_\downarrow - E_\uparrow)}{1.85\times10^{-4} eVK^{-1}}$$

For CoSi, our calculations give an energy difference of 0.85704 eV for the (0 -1 1) C configuration. Therefore, the estimated Curie temperature of the slab in configuration C is $T_c = 2460\ K$. It has been shown that MFA tends to overestimate the Curie temperatures[31,33,34] (18 times larger in MnSi thin films[31]). Nevertheless, results are intended to present the existence of a ferromagnetic phase in a CoSi slab and not for the exact calculation of the Curie temperature. To understand the effects of Mn doping in a (0 -1 1) CoMnSi surface, one Co atom was replaced on each supercell with a Mn atom. This gives a doping level of approximately 2.5%. Figure 8 presents the calculated Curie temperature for CoMnSi, changing the position of the Mn atom through the supercell. The results suggest that the inclusion of Mn can improve the remnant magnetic moment of the CoMnSi nanowires without ordered vacancies, but the presence of vacancies is needed to increase the Curie temperature to values over 800K. For T_c >800K the interaction of the Mn atoms with the conduction electrons at the nanowire boundaries and vacancies, leaves the supercell atom with a considerable higher magnetic moment compared to the undoped case. Results show that replacing the Co atoms at the core with Mn on the already ferromagnetic configuration could slightly improve or reduce the magnetic phase of the CoMnSi nanowire. Thus, the presence of the vacancies still holds an important role on the magnetic configuration to form. These vacancies could help the formation of localized magnetic moments on the Co atoms as one can see in Figure 5, which indicates a higher magnetic moment for atoms placed near the vacancy. As mentioned before, the overestimation of the Curie temperatures shown in Figure 8 is a well know problem when using MFA.

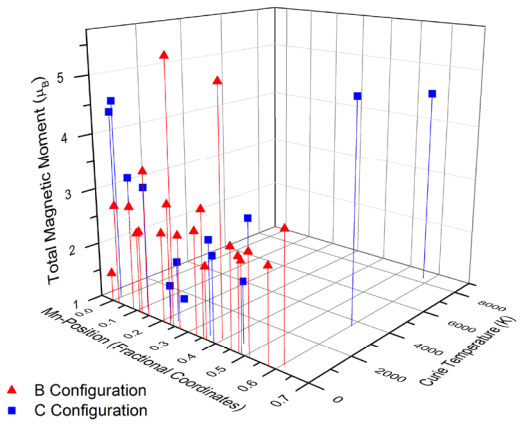

FIG. 8. Curie temperature of the B and C supercell configuration (see Figure 5) as a function of the Mn atom position and the total magnetic moment of the supercell. 0 values of the Curie temperature correspond to a non-ferromagnetic configuration.

To confirm the magnetic moment per Co atom on the as grown CoSi nanowires and to compare with the ~1μ_B obtained in the DFT calculations, measurements of the magnetization over a single CoSi nanowire were obtained in the TEM using a phase retrieval method called Off-axis electron holography (EH). EH is an interferometric technique were two images (reference and object) are combined and postprocessed on Fourier space to retrieve the phase shift of the electron wave after interacting with the sample.[35] The most interesting feature of the image collected (holograms), as the one shown in Fig. 9a, are the

presence of interference fringes caused by the wire, below the sample plane, biased at a fixed DC voltage. To get reliable magnetization measurements magnetic and crystalline phase contributions need to be separated from two different electron holograms with opposite magnetization directions. The in-situ magnetization procedure inside the TEM relies in using the Objective Lens as an external magnetic field source and tilting the nanowire to facilitate the magnetization over its long axis[36]. In this way, Figure 9b presents the magnetic contribution obtained after performing the in-situ magnetic reversal procedure, a phase jump (color change) over the two regions on the vicinity of the wire is noticeable. From the gradient of the magnetic phase contribution, the lines in Figure 9c represent the flux within with a color wheel as an inset to assign it a direction.

From the phase shift (Δφ) in Figure 9d, the magnetization can be calculated using the equation: $M = \frac{\bar{h}\cdot\Delta\varphi}{2\pi\, e\cdot\mu_0\cdot S}$, where 'S' is the cross section of the nanowire and μ_0, e and $\bar{h}$ are constants. The magnetic flux density follows with: $B = \left(\bar{h}/e\cdot t\right)\cdot {}^{\delta\varphi}/_{dx}$, using the section thickness 't'[37]. From the phase shift of approximately 6.1 radians the magnetic induction was quantitatively evaluated as B = 1.37 T. The average magnetic moment per cobalt atom can be estimated considering that $\mu = \frac{M_{mole}}{N_A}\frac{B}{\rho}\gamma$, where Υ is the fraction of cobalt atoms and M_{mole} the molecular weight of cobalt silicide. The obtained magnetic moment per Co atom in the CoSi nanowire is 1.2 μ_B. The observed vortex patterns are size related.

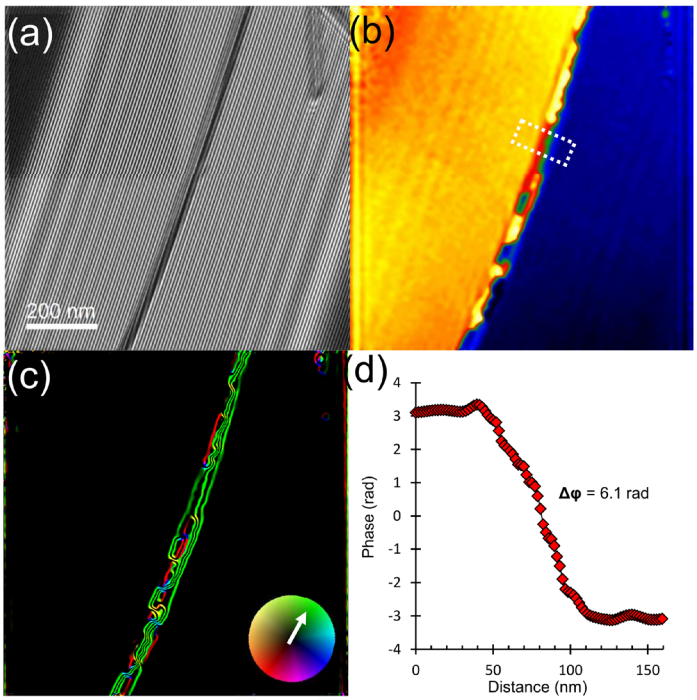

FIG. 9. (a) Electron hologram of the CoSi NW selected for EH, (b) Magnetic contribution obtained after subtracting two phase images with opposite remnant magnetization, (c) magnetic contour image, (d) phase profile of the region highlighted in (b) showing the phase jump between the two regions of the nanowire.

IV. CONCLUSIONS

We synthesized for the first-time high quality $Co_{1-x}Mn_xSi$ (x=0 – 0.026) nanowires with high yields which exhibit a Curie temperature above 800K for the x=0.026 case. DFT calculations support the magnetic enhancement that Mn atoms cause on a (0 -1 1) super cell of the semimetal CoSi. Its magnetic behavior can be explained in terms of the RKKY exchange interaction between the Mn electrons and the conduction electrons of the semimetal. Magnetic electron holography was made on nanowires to give more information about the magnetic field distribution in the nanowire and to confirm the results of the calculated magnetization per Co-atom in CoSi nanowires. The magnetic hysteresis curves confirm a significant enhancement of the room temperature remanent magnetization via Mn-doping and the DFT results clarifies the role of the vacancies to achieve the high Curie temperatures observed in CoMnSi nanowires. Such a high Curie temperature Si-based nanowires are promising candidates in high temperature spintronic applications.

V. ACKNOWLEDGEMENTS

Work partially supported by NSF Grant HRF-1736093.The DFT calculations were performed using the facilities of Holland Computer, University of Nebraska – Lincoln. A. R. R. acknowledges support from Puerto Rico NASA Space Consortium NNX15A11IH, NSF PR-LSAMP Grant HRD1139888, and thanks Dr. Renat Sabirianov, University of Nebraska - Omaha for facilitating the access to the facilities and helpful discussions. The electron microscopy work was performed in the Kleberg Advanced Microscopy Center (KAMC) and supported by the National Institute on Minority Health and Health Disparities (G12MD007591) from the National Institutes of Health.

VI. REFERENCES

1 J. F. DiTusa, in *Handbook of Spintronics*, edited by Y. Xu, D. D. Awschalom, and J. Nitta (Springer Netherlands, Dordrecht, 2016), p. 523.
2 K. Seo, H. Yoon, S.-W. Ryu, S. Lee, Y. Jo, M.-H. Jung, J. Kim, Y.-K. Choi, and B. Kim, ACS Nano **4,** 2569 (2010).
3 K. Seo, K. S. K. Varadwaj, P. Mohanty, S. Lee, Y. Jo, M.-H. Jung, J. Kim, and B. Kim, Nano Letters **7,** 1240 (2007).
4 K. Seo, N. Bagkar, S.-i. Kim, J. In, H. Yoon, Y. Jo, and B. Kim, Nano Letters **10,** 3643 (2010).
5 J. In, K. S. K. Varadwaj, K. Seo, S. Lee, Y. Jo, M.-H. Jung, J. Kim, and B. Kim, The Journal of Physical Chemistry C **112,** 4748 (2008).
6 M.-H. Hung, C.-Y. Wang, J. Tang, C.-C. Lin, T.-C. Hou, X. Jiang, K. L. Wang, and L.-J. Chen, ACS Nano **6,** 4884 (2012).
7 M. Jourdan, J. Minar, J. Braun, A. Kronenberg, S. Chadov, B. Balke, A. Gloskovskii, M. Kolbe, H. J. Elmers, G. Schonhense, H. Ebert, C. Felser, and M. Klaui, Nat Commun **5,** 3974 (2014).
8 D. Shinoda, physica status solidi (a) **11,** 129 (1972).
9 T.-K. Liu, S.-H. Chiou, J. van Lierop, and C. Ouyang, RSC Advances **6,** 23634 (2016).

[10] L. Sun, Y. Hao, C. L. Chien, and P. C. Searson, IBM Journal of Research and Development **49,** 79 (2005).
[11] K. Gandha, K. Elkins, N. Poudyal, X. Liu, and J. P. Liu, Scientific Reports **4,** 5345 (2014).
[12] Y. P. Ivanov, A. Chuvilin, S. Lopatin, and J. Kosel, ACS Nano **10,** 5326 (2016).
[13] E. Ortega, S. M. Reddy, I. Betancourt, S. Roughani, B. J. H. Stadler, and A. Ponce, Journal of Materials Chemistry C **5,** 7546 (2017).
[14] K. Seo, S. Lee, H. Yoon, J. In, K. S. K. Varadwaj, Y. Jo, M.-H. Jung, J. Kim, and B. Kim, ACS Nano **3,** 1145 (2009).
[15] Y.-H. Liang, S.-Y. Yu, C.-L. Hsin, C.-W. Huang, and W.-W. Wu, Journal of Applied Physics **110,** 074302 (2011).
[16] C.-I. Tsai, P.-H. Yeh, C.-Y. Wang, H.-W. Wu, U.-S. Chen, M.-Y. Lu, W.-W. Wu, L.-J. Chen, and Z.-L. Wang, Crystal Growth & Design **9,** 4514 (2009).
[17] A. L. Schmitt, L. Zhu, D. Schmeiβer, F. J. Himpsel, and S. Jin, The Journal of Physical Chemistry B **110,** 18142 (2006).
[18] C.-M. Lu, H.-F. Hsu, and K.-C. Lu, Nanoscale Research Letters **8,** 308 (2013).
[19] A. E. van Arkel and J. H. de Boer, Zeitschrift für anorganische und allgemeine Chemie **148,** 345 (1925).
[20] S. Meschel and O. J. Kleppa, *The Standard Enthalpies of Formation of Some 3d Transition Metal Aluminides by High-Temperature Direct Synthesis Calorimetry* (1994).
[21] S. Pearton, Nature Materials **3,** 203 (2004).
[22] M. A. Majidi, A. Bupu, and A. D. Fauzi, Physica B: Condensed Matter **526,** 172 (2017).
[23] K. Yosida, *Theory of Magnetism* (Springer-Verlag Berlin Heidelberg, 1996).
[24] K. Yosida, Physical Review **106,** 893 (1957).
[25] M. S. Lataifeh, M. Oshea, A. S. Saleh, and S. H. Mahmood, arXiv preprint arXiv:1711.03052 (2017).
[26] Y. Yeshurun, M. B. Salamon, K. V. Rao, and H. S. Chen, Physical Review Letters **45,** 1366 (1980).
[27] G. Kresse and J. Hafner, Physical Review B **47,** 558 (1993).
[28] G. Kresse and J. Furthmüller, Computational Materials Science **6,** 15 (1996).
[29] G. Kresse and J. Furthmüller, Physical Review B **54,** 11169 (1996).
[30] P. E. Blöchl, Physical Review B **50,** 17953 (1994).
[31] M. Hortamani, L. Sandratskii, P. Kratzer, I. Mertig, and M. Scheffler, Physical Review B **78,** 104402 (2008).
[32] S. Datta, C. Trindle, and F. Illas, *Theoretical and Computational Aspects of Magnetic Organic Molecules* (2014).
[33] J. Rusz, L. Bergqvist, J. Kudrnovský, and I. Turek, Physical Review B **73,** 214412 (2006).
[34] K. Sato, W. Schweika, P. H. Dederichs, and H. Katayama-Yoshida, Physical Review B **70,** 201202 (2004).
[35] E. Völkl, L. F. Allard, and D. C. Joy, *Introduction to Electron Holography* (Kluwer Academic/Plenum Publishers, 1999).
[36] J. Cantu-Valle, I. Betancourt, J. Sanchez, F. Ruiz-Zepeda, M. Maqableh, F. Mendoza-Santoyo, B. Stadler, and A. Ponce, *Mapping the magnetic and crystal structure in cobalt nanowires*, Vol. 118 (2015).
[37] J. Cantu-Valle, E. Díaz Barriga-Castro, V. Vega, J. García, R. Mendoza-Reséndez, C. Luna, V. Manuel Prida, K. Nielsch, F. Mendoza-Santoyo, M. Jose-Yacaman, and A. Ponce, Journal of Magnetism and Magnetic Materials **379,** 294 (2015).